ACS APPLIED MATERIALS & INTERFACES

Research Article

www.acsami.org

Solution Processed Al-Doped ZnO Nanoparticles/TiOx Composite for Highly Efficient Inverted Organic Solar Cells

Abay Gadisa,*[,†,‡] Travis Hairfield,[‡] Leila Alibabaei,[†] Carrie L. Donley,[§] Edward T. Samulski,[†] and Rene Lopez[‡]

[†]Department of Chemistry, University of North Carolina at Chapel Hill, Caudill and Kenan Laboratories CB 3290, Chapel Hill, North Carolina 27599, United States

[‡]Department of Physics and Astronomy, University of North Carolina at Chapel Hill, Phillips Hall CB 3255, Chapel Hill, North Carolina 27599, United States

[§]Chapel Hill Analytical and Nanofabrication Laboratory, University of North Carolina at Chapel Hill, Chapman Hall CB 3216, Chapel Hill, North Carolina 27599, United States

Supporting Information

ABSTRACT: We investigated the electrical properties of solution processed Al-doped ZnO (AZO) nanoparticles, stabilized by mixing with a TiOx complex. Thin solid films cast from the solution of AZO-TiOx (AZOTi) (Ti/Zn ~0.4 in the bulk and ~0.8 on its surface) is processable in inert environment, without a need for either ambient air exposure for hydrolysis or high temperature thermal annealing commonly applied to buffer layers of most metal-oxides. It was found that the electronic structure of AZOTi matches the electronic structure of several electron acceptor and donor materials used in organic electronic devices, such as solar cells. Inverted solar cells employing a bulk heterojunction film of poly(3-hexylthiophene) and phenyl-C61-butyric acid methyl ester, cast on an indium−tin-oxide/AZOTi electrode, and capped with a tungsten oxide/aluminum back electrode, give rise to a nearly 70% fill factor and an optimized open-circuit voltage as a result of efficient hole blocking behavior of AZOTi. The resulting electron collecting/blocking capability of this material solves crucial interfacial recombination issues commonly observed at the organic/metal-oxide interface in most inverted organic bulk heterojunction solar cells.

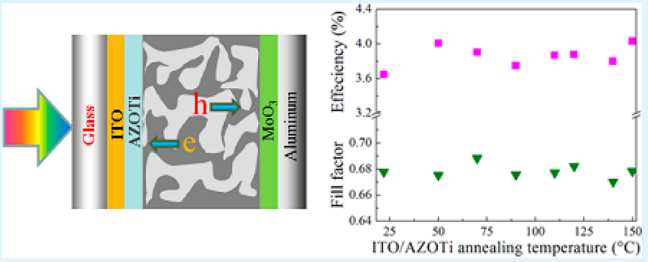

KEYWORDS: *interface modification, metal-oxide, AZO, solar cell, work function*

1. INTRODUCTION

In recent years, rapid progress has been made in the development of materials for polymer/fullerene bulk heterojunction (BHJ) organic solar cells. In particular, the emergence of efficient, low-bandgap materials and new device designs have resulted in highly efficient solar cells.[1−4] Inverted polymer/fullerene BHJ solar cells have been growing in appeal because of their ease of fabrication, long lifespan[5], and high efficiency.[1−3] The core electrode in BHJ solar cells is usually based on indium−tin−oxide (ITO), which is typically coated with buffer layers to tune its work function[1−6] or reduce its roughness. In inverted solar cells, these metal-oxide buffer layers, formed either through thermal evaporation or solution processing, are crucial elements in collecting/blocking free charges under device operation conditions.[1−6] Solution processed metal-oxide films are an attractive way to form the buffer layers since these are well suited for large area fabrication using cheap technologies like roll-to-roll printing. For this reason, sol−gel routes to several types of metal-oxides (e.g., titanium oxide (TiOx),[7] zinc oxide (ZnO),[8] molybdenum oxide (MoOx),[9] and vanadium oxide (V_2O_5)[10]) have been targeted for application in organic solar cells. On occasion, the optimization of such electron transporting metal-oxide buffer layers also requires additional interfacial modification to reduce losses originating at metal-oxide/organic interfaces. For example, inverted solar cells incorporating an optically thin interlayer of a conjugated polyelectrolyte,[11] an alcohol/water-soluble conjugated polymer,[12] or a dye[6] on top of their ITO/metal-oxide electrodes showed enhanced performance stemming from the apparent modification of surface properties and electronic structure.

Multilayer electrodes and/or numerous steps should be avoided to fabricate cost-effective and practical photovoltaic devices. For example, room temperature processable metal-oxides are ideal materials for developing efficient and stable single layer and multilayer organic solar cells though several commonly employed metal-oxide interlayers such as ZnO demand post-thermal annealing to attain improved conductiv-

Received: May 13, 2013
Accepted: August 15, 2013
Published: August 27, 2013

ity.[2,5,8] Such high temperature processing is a drawback for realizing competitive organic solar cells. In particular, high temperature procedures commonly applied to thin films of most metal-oxide buffer layers are typically not compatible with most organic photoactive films because of polymer degradation issues. In addition, such annealing processes limited the fabrication of flexible organic solar cells on plastic substrates. There is another general limitation of multilayer solar cells employing metal-oxide buffer layers: metal-oxides that can be processed in inert glove boxes are uncommon because they require oxidation steps. However this is a preferable fabrication step since most organic films need to be processed in such inert environments. Only inverted solar cells with ZnO nanoparticle buffer layers have been processed either in glovebox or air without showing significant differences.[13]

Here, we report fabrication of efficient inverted single and tandem BHJ solar cells employing a buffer layer fabricated from Al-doped zinc oxide nanoparticles 20−40 nm in size, dispersed in a TiOx complex containing solution. The TiOx was originally added to stabilize the AZO nanoparticle dispersion. The nanoparticle dispersion gives rise to a Ti/Zn atomic concentration ratio of ∼0.4 in the bulk, and ∼0.8 on the surface of spin-cast solid films. This metal-oxide composition, called AZOTi, has two important elements that benefit production of low cost devices. Its functionality is easily optimized through annealing at very low temperatures; nonannealed films worked efficiently as well. Second, the annealing steps can be carried out equally effectively in an inert atmosphere. Furthermore, in inverted solar cells the AZOTi buffer layers cast on an ITO electrode give rise to optimized photovoltaic activity without a need for any interface modification. Solar cells incorporating a BHJ film of poly(3-hexylthiophene) (P3HT) and phenyl-C61-butyric acid methyl ester (PCBM) exhibited an open-circuit voltage exceeding 0.63 V and a nearly 70% fill factor, irrespective of the annealing conditions for the AZOTi buffer layer. These characteristics of AZOTi effectively circumvent the processing limitations of most organic films and flexible substrates thereby classifying AZOTi as a material of choice for fabrication of cheap, efficient and stable inverted single junction and tandem BHJ solar cells, as well as flexible electronic devices.

2. EXPERIMENTAL SECTION

Solar Cell Fabrication. An AZOTi nanoparticle dispersion in dimethylbenzene (with 10 wt. % AZO) was delivered by NanoAmor. A TiOx complex was originally added into the solution of Al-doped ZnO nanoparticles to stabilize the nanoparticle dispersion. The AZOTi solution was diluted to desired concentration (2 wt. %) by adding ethanol. AZOTi films were formed by spin-casting from the diluted solution on a precleaned indium−tin-oxide electrode at a spin-speed of 3500 rpm (without ramping). The ITO substrates were ultrasonic cleaned with deteregent, acetone and isoproyl alcohol. The ITO/AZOTi films were transferred to a nitrogen-filled glovebox and annealed at various temperatures. P3HT/PCBM (1:0.8, wt. %) was prepared in 1,2-dichlorobenzene with a polymer concentration of 10 mg/mL. About 100 nm P3HT/PCBM BHJ films were formed on ITO/AZOTi substrates by spin-casting the organic solution at a spin-speed of 450 rpm. Partially wet samples were kept in Petri dishes for 10 min, and subsequently thermally annealed at 140 °C for 5 min. Slow-grown P3HT/PCBM films were also spin-cast at 450 rpm for 60 s and kept in closed Petri dishes for about 2 h. PTB7-F20 (polythienothiophene-co-benzodithiophenes 7 F-20), and phenyl-C71-butyric acid methyl ester ($PC_{70}BM$) based solar cells were fabricated by spin-casting PTB7-F20/$PC_{70}BM$ (1:1.5) from a chlorobenzene solution with a 10 mg/mL polymer concentration, and contains 3 vol.% 1,8-diiodooctane. Finally, 10 nm of MoO_3 and 100 nm of Al were subsequently thermally evaporated on the organic film in a vacuum evaporator located within the glovebox. Tandem cells comprising P3HT/PCBM in the front cell and the bulk heterojunction blend of poly [2,1,3-benzothiadiazole-4,7-diyl [4,4-bis(2-ethylhexyl)-4H-cyclopenta[2,1-b:3,4-b′]dithiophene-2,6-diyl]] (PCPDTBT) and $PC_{70}BM$ in the back cell were fabricated. The front P3HT/PCBM cell was made by following the recipe of the single layer inverted P3HT/PCBM cell, subjected to thermal annealing. Then the first separation/recombination layer was made by spin-casting poly(3,4-ethylenedioxythiophene) poly(styrenesulfonate) (PEDOT:PSS) (Clevios PH 500) on top of the P3HT/PCBM layer. A fluorosurfactant Zonyl FS-300 (0.5 vol.%) was added to the water dispersion of PH 500 to enhance its wettability while Dimethyl sulfoxide (5 vol.%) was added to increase the conductivity of the PH 500 solid film. After spin-casting the PH 500, the device was annealed in glovebox at 140 °C for 10 min. This was followed by spin-casting AZOTi and another thermal annealing at 150 °C for 10 min. This was followed by spin-casting PCPDTBT/$PC_{70}BM$ (1:3) from a chlorobenzene solution with a polymer concentration of 7 mg/mL. The tandem device was completed after thermally evaporating a 10 nm of MoO3 and 100 nm of Al. All device annealing processes and photovoltaic measurements were made in a nitrogen-filled glovebox.

Photovoltaic Measurements. Current−voltage measurements were performed using a Keithley 2400 source meter. The photovoltaic characteristics of the solar cells were recorded under a simulated A.M. 1.5G (1000 W/m^2) solar illumination from a Newport solar simulator.

UPS and XPS Measurements. Ultraviolet photoemission spectroscopy measurements were performed using the He I photon line ($h\nu$ = 21.22 eV) of a He discharge lamp attached to a Kratos Asis Ultra DLD X-ray photoelectron spectrometer with a base pressure of 3 × 10^{-9} Torr. Hemispherical analyzer with the analyzer pass energy set to 5 eV was used to collect emitted photoelectrons. The onset of the photoemission spectra, which is used to determine the position of the vacuum level, was measured after applying a bias of −5 V. X-ray photoemission spectroscopy was carried out with the AlKα line ($h\nu$ = 1486.6 eV) with an analyzer pass energy of 20 eV for high resolution scans and 80 eV for survey scans. All spectra were corrected to the C 1s peak at 284.6 eV and the Zn 2p and Ti 2p spectra were fit using Shirley backgrounds and mixed Lorentzian−Gaussian functions.

3. RESULTS AND DISCUSSION

3.1. Composition and Electronic Properties. To investigate the processability limits of AZOTi, spin-cast thin films were thermally annealed at various temperatures (22−150 °C). The composition of AZOTi films cast on ITO was characterized by X-ray photoelectron spectroscopy (XPS). In the XPS spectra, as depicted in Figure 1, Zn, O, Al, and Ti are clearly observed. High resolution scans of the Zn 2p and Ti 2p region are shown in the right panel of Figure 1, and the corresponding peak positions are displayed in Table 1. The Zn $2p_{3/2}$ peak position of ∼1021.2 eV along with the binding energy of the Zn Auger peak indicates the presence of Zn^{2+}.[14] Similarly, the Ti $2p_{3/2}$ peak position of ∼458.0 eV coincides with the binding energy values of Ti^{4+} in TiO_2.[15] The XPS analysis also provides the ratio of Ti to Zn atomic concentrations which is found to be ∼0.80 for all samples (See Table 1). Since XPS is a surface sensitive characterization technique the high Ti/Zn ratio may not represent the bulk composition of the metal-oxide film. Hence we employed energy-dispersive spectroscopy (EDS) to make elemental analysis throughout the whole film. The elemental compositions of the nonannealed sample and the sample annealed at 150 °C are similar as determined by the analysis of EDS spectra (See Supporting Information, Figure S1). According to the data extracted from EDS, the Ti/Zn atomic concentration ratio in the nanoparticles is ∼0.4. Taking the XPS and EDS analysis

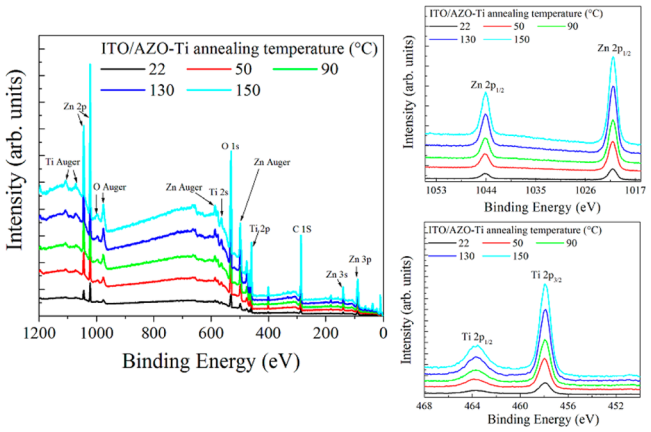

Figure 1. X-ray photoelectron spectroscopy (XPS) spectra of AZOTi spin-cast on an indium−tin-oxide electrode. The Zn and Ti peaks are shown on the right figures. The spectra are vertically offset for clarity.

Table 1. XPS Characteristics of ITO/AZOTi Substrates Annealed in a Glove Box

AZOTi annealing temperature (°C)	$2p_{3/2}$ (eV)		Ti/Zn atomic concentration ratio
	Zn	Ti	
nonannealed	1021.08	457.93	0.82
50	1021.14	458.00	0.81
90	1021.20	458.07	0.83
130	1021.24	458.10	0.83
150	1021.23	458.12	0.82

together, we conclude that the surface is rich in Ti complexes, while the bulk is dominated by the ZnO complexes.

The electronic structure of semiconducting oxides plays a major role in the performance of electronic devices that employ them in electrodes. For example, in photovoltaic devices utilizing such metal-oxides, wider band-gaps are preferred for excellent optical transmission. Concurrently, the matching of the valence and conduction bands of the metal-oxides with the frontier energy levels of organic semiconductors is desired for loss-free charge injection/collection processes. We have investigated the electronic structure of the AZOTi samples using ultraviolet photoelectron spectroscopy (UPS) (Figure 2). It was observed that the ionization potential and work function of the oxide films slightly change with annealing temperature as shown in Table 2. Considering the electronic properties of the nonannealed device as a reference, a work function increase of

Table 2. Ionization Potential and Work Function of ITO/AZOTi Substrates Annealed at Various Temperatures in a Nitrogen-Filled Glove Box[a]

AZOTi annealing temperature (°C)	ionization potential (eV)	work function (eV)
Nonannealed	6.85	3.07
50	6.87	3.11
90	7.00	3.25
130	7.05	3.31
150	7.12	3.33

[a]These parameters were extracted from the UPS spectra depicted in Figure 2.

40, 180, 240, and 260 meV was measured after thermal annealing at a temperature of 50, 90, 130, and 150 °C, respectively. It should be noted that this change is predominately due to a shift in the secondary electron cutoff, which indicates a shift in the vacuum level. This progressive increase in work function may be attributed to slight surface morphological or chemical changes incurring during the annealing process.

In general, the UPS measurements reveal that thin AZOTi films spin-cast on ITO are characterized by lower surface work functions compared to our previously reported work function value (3.78 eV for Al-doped ZnO grown by pulsed laser deposition technique).[6] Typical work function values of AZO films prepared by various techniques fall in the range of 3.7−4.6 eV,[16] although a work function of 3.2 eV was reported for sputter-deposited AZO.[17] The work function of AZO is greatly influenced by the Al-doping concentration, while film preparation methods also play a crucial role as well.[16] For films studied here, both the XPS Al/Zn, and O/Zn atomic concentration ratio slightly decrease as the AZOTi thermal annealing temperature increases (See Table S1 in Supporting Information). X. Jiang et al. have shown that by decreasing the surface O/Zn atomic concentration ratio from 1.67 to 0.84, the surface work function of AZO increased from 3.7 to 4.4 eV,[16] empirically demonstrating that the presence of more oxygen atoms on surface leads to a lowering of the surface work function. For the samples considered in our study, we calculated the O/(Ti+Zn) ratio to compare it with the work by Jiang and co-workers. We found that this ratio decreased from 2.90 to 2.55, that is, the samples in this study contain more surface oxygen than those reported by Jiang and co-workers,[16] but a similar correlation between work function and surface oxygen concentration is observed. On the other hand, carbon contamination at the film surface is also known to

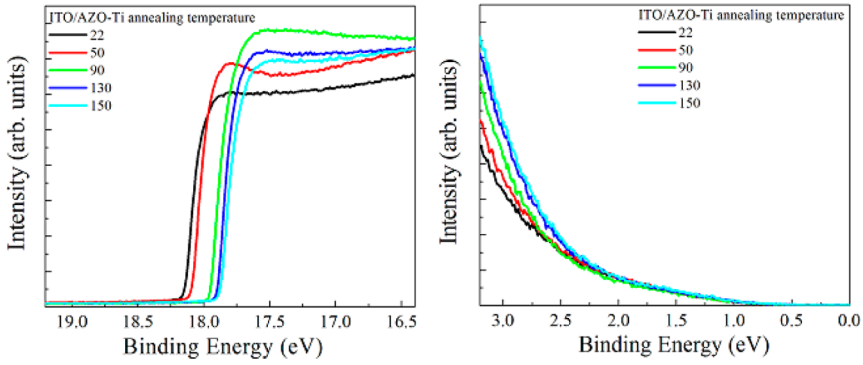

Figure 2. UPS spectra of AZOTi film spin-cast on ITO. The oxide films were annealed at various temperatures under inert environment.

significantly affect surface work functions.[18,19] For the devices studied here, the carbon contamination follows the trend of oxygen enrichment at the surface (See Supporting Information Table S1). Overall, the slight change in work function with device type may be the result of both effects, some surface carbon contamination and oxygen enrichment.

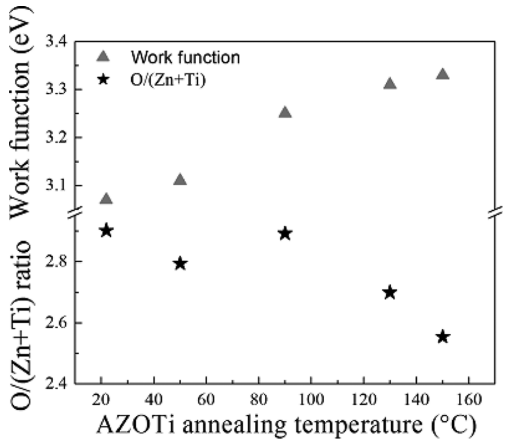

Figure 3. Trends of O/(Zn + Ti) ratio and the work function of AZOTi films.

3.2. Photovoltaic Properties of Inverted Solar Cells.

Inverted photovoltaic devices were made on ITO/AZOTi substrates by spin-casting BHJ films of P3HT and PCBM. The ITO/AZOTi electrode collects the photogenerated electrons while a MoO_3/Al electrode evaporated on top of the active layers collects the photogenerated holes. The photovoltaic parameters of the solar cells barely show any differences upon changing the thermal treatment conditions of ITO/AZOTi electrodes (Figure 4). This is a remarkable result showing that excellent charge collection and blocking efficiencies have been achieved in all devices regardless of thermal treatment protocols. To highlight how important this result is, one can consider current alternatives: ZnO is a commonly used buffer layer in inverted single layer[2,5] as well as record-efficiency-holding tandem solar cells.[4] However, in all of these efficient inverted devices, ZnO needs to be annealed at a temperature of 150−300 °C[4,5,20] to optimize its conductivity. An interfacial layer of TiOx cast on ITO can be optimized by storing the films overnight at room temperature.[7] A TiOx precursor can also be converted to a solid-sate film upon annealing in air.[21] This type of processing is not compatible with the processing of most organic films, which usually takes place in inert environments such as a nitrogen filled glovebox.

In general, the AZOTi buffer layer is an ideal choice for inverted organic solar cells because of its excellent functionality even without any annealing and because its interface qualities are not substantially modified when it is annealed in inert environment. As depicted in Figure 4, the average fill factor of all device types stays close to 70%, which is the highest value commonly achieved in P3HT/PCBM-based photovoltaic devices.[21,22] This is attributed to good charge collection/blocking efficiency at both electrodes, as well as excellent charge transport within the BHJ film. Simultaneously, the open-circuit voltage has attained the optimum value associated with P3HT/PCBM-based solar cells. In other words, the concurrent optimization of the fill factor and the open-circuit voltage implies that both electrodes have made ohmic contacts and impose no unwanted interfacial series resistances. Recently, the Heeger group noticed that a reduction of the work function of ITO/ZnO by overlaying a thin layer of polyethylenimine (80% ethoxylated) on top of ZnO leads to increased photocurrent and fill factor in a small molecule/fullerene bulk heterojunction solar cell.[23] These increases were assumed to originate from a reduction of charge-carrier trap-assisted recombination because of the increased built-in potential and internal electric field coming from a reduced work function of cathode. We believe that the same hypothesis applies to the ITO/AZOTi-based inverted solar cells. On the other hand, the exact role of TiOx in the electronic property of AZOTi is not clear. However, previous reports have suggested that TiOx mixed with ZnO primarily alleviates interfacial recombination through fill-up of ZnO surface traps by electrons from amorphous TiOx.[24]

The postfilm production thermal annealing of the ITO/AZOTi/P3HT/PCBM at 140 °C may seem to weaken our argument regarding the optimization of AZOTi's functionality with or without low temperature thermal annealing. For this reason we have also fabricated inverted solar cells comprising nonannealed P3HT/PCBM BHJ films. To optimize the morphology of the P3HT/PCBM film, a slow-growth method[22b] has been employed (see Experimental Section for details). The photovoltaic performance of the corresponding solar cells is compiled in Table 3. It is clearly evident that the solar cells perform nearly equally well irrespective of the different thermal treatment protocols on the AZOTi layers.

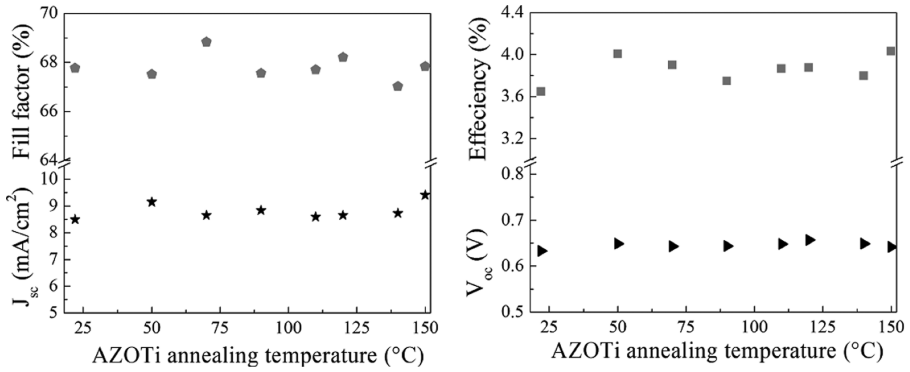

Figure 4. Photovoltaic parameters of ITO/AZOTi/P3HT/PCBM/MoO_3/Al inverted solar cells. The left figure shows the short-circuit current (J_{sc}) and fill factor while the right panel displays the open-circuit voltage (V_{oc}) and power conversion efficiency as a function of the ITO/AZOTi annealing temperature.

Table 3. Photovoltaic Parameters of Inverted Solar Cells Comprising Slow-Grown and Thermally Nonannealed P3HT:PCBM Films

AZOTi annealing temperature (°C)	J_{sc} (mA/cm^2)	V_{oc} (V)	FF (%)	efficiency (%)
nonannealed	8.52	0.62	61.76	3.19
90	8.26	0.62	61.35	3.14
130	8.76	0.61	60.54	3.24
150	8.29	0.62	63.74	3.28

Compared to the samples treated by post-thermal annealing, the slow grown samples give rise to smaller fill factors. This issue was previously attributed to solvent traces in the photoactive film, and it was solved through thermal annealing of the slow-grown film at mild temperature (typically 110 °C).[22b]

We have also fabricated inverted solar cells with PTB7-F20/$PC_{70}BM$ BHJ film, sandwiched between ITO/AZOTi and MoO_3/Al electrodes. PTB7-F20 is a class of novel low bandgap polymers, which gives rise to substantially high power conversion efficiency in solar cells, without a need for thermal treatment.[25,26] Our results show that PTB7-F20/$PC_{70}BM$-based solar cells also show negligible differences for devices comprising ITO/AZOTi substrates annealed at different temperatures (See Figure S2 in Supporting Information).

After successful utilization of AZOTi in the fabrication of optimized single layer P3HT/PCBM-inverted solar cells, we also fabricated tandem cells comprising ITO/AZOTi/P3HT/PCBM in the front cell and a blend of a low band gap polymer [2,1,3-benzothiadiazole-4,7-diyl [4,4-bis(2-ethylhexyl)-4H-cyclopenta[2,1-b:3,4-b′]dithiophene-2,6-diyl]] (PCPDTBT) and $PC_{70}BM$ as an active layer in the back cell. The two subcells were separated by a bilayer of PEDOT:PSS/AZOTi. While the hole-conducting PEDOT:PSS extracts holes from the front cell, the overlaying AZOTi transports electrons from the back cell toward the PEDOT:PSS/AZOTi charge recombination center. The current–voltage characteristics of a typical prototype inverted tandem cell and single cells are displayed in Figure 5.

The performance of the solar cells were evaluated by extracting the short-circuit current (J_{sc}), open circuit-voltage (V_{oc}), fill factor (FF), and power conversion efficiency (μ) from the current–voltage characteristics depicted in Figure 5. The

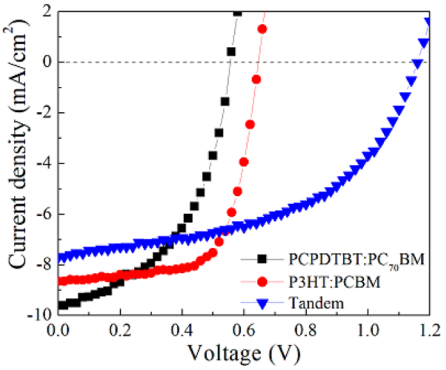

Figure 5. Current voltage characteristics of typical inverted single cells comprising P3HT/PCBM and PCPDTBT/$PC_{70}BM$ active layers as well as a tandem solar cell with an ITO/AZOTi/P3HT/PCBM bottom cell and PEDOT:PSS/AZOTi/PCPDTBT/$PC_{70}BM$/MoO_3/Al top cell.

P3HT/PCBM single cells shows J_{sc} = 8.66 mA/cm^2, V_{oc} = 0.65 V, FF = 68%, and μ = 3.83%, while the PCPDTBT/$PC_{70}BM$ single cell gives J_{sc} = 9.62 mA/cm^2, V_{OC} = 0.55 V, FF = 50%, and μ = 2.65%. The tandem cell yields J_{sc} = 7.71 mA/cm^2, V_{oc} = 1.18 V, FF = 50%, and μ = 4.55%. An optimized noninverted tandem cell comprising similar subcells, but with a different separation layer, yields an efficiency of 6.5%.[21] Herein our aim is to demonstrate the functionality of AZOTi in inverted tandem cells; fabricating optimized tandem devices is outside of the scope of this report. Recently, N. Li et al. demonstrated efficient single layer and tandem solar cells utilizing solution processed Al-doped ZnO and a low conductivity PEDOT:PSS.[27] In the later report, thermal annealing was applied to optimize the functionality of the oxide interlayer.

4. CONCLUSIONS

Al-doped ZnO nanoparticles, dispersed in a TiOx complex comprising solution, show excellent electrical behavior in inverted solar cells comprising P3HT/PCBM bulk heterojunction films. Moreover, the AZOTi film is readily optimized by processing in inert environments at low thermal annealing temperatures. This efficient charge collecting/blocking electrode has resulted in highly efficient P3HT/PCBM-based inverted photovoltaic devices, characterized by optimum fill factors and open-circuit voltages without a need for additional interface modifications. AZOTi was also successfully applied for fabrication of proto-type tandem cells and inverted solar cells with PTB7-F20/$PC_{70}BM$ photoactive layer. On the basis of UPS measurements, AZOTi buffer layers applied on ITO electrode have an exceptionally low surface work function that is mainly attributed to the oxygen enrichment of the film surfaces. The low work function is a key to blocking holes at the electron collecting interface. The latter contributes to the elimination of interface recombination and enhances fill factor.

■ ASSOCIATED CONTENT

Supporting Information

EDS spectra of nonannealed and annealed ITO/AZOTi substrates, the elemental composition of AZOTi, analyzed by XPS, and photovoltaic data of ITO/AZOTi/PTB7-F20/$PC_{70}BM$/MoO_3/Al. This material is available free of charge via the Internet at http://pubs.acs.org.

■ AUTHOR INFORMATION

Corresponding Author

*E-mail: abay@unc.edu, abaymy@yahoo.com.

Notes

The authors declare no competing financial interest.

■ ACKNOWLEDGMENTS

Support for this work from NSF (Solar: DMR-0934433) is gratefully acknowledged. L.A. wishes to acknowledge financial support from the Research Triangle Solar Fuels Institute (RTSFI), a consortium consisting of RTI International, Duke University, North Carolina State University, and the University of North Carolina at Chapel Hill.

■ REFERENCES

(1) He, Z.; Zhong, C.; Su, S.; Xu, M.; Wu, H.; Cao, Y. *Nat. Photon.* **2012**, *6*, 591–595.

(2) Small, C. E.; Chen, S.; Subbiah, J.; Amb, C. M.; Tsang, S.-W.; Lai, T.-H. S.-W.; Reynolds, J. R.; So, F. *Nat. Photon.* **2012**, *6*, 115–120.

(3) Li, G.; Zhu, R.; Yang, Y. *Nat. Photon.* **2012**, *6*, 153−161.
(4) You, J.; Dou, L.; Yoshimura, K.; Kato, T.; Ohya, K.; Moriarty, T.; Emery, K.; Chen, C. C.; Gao, J.; Li, G.; Yang, Y. *Nat. Commun.* **2013**, *4*, 1446−1455.
(5) Sun, Y.; Seo, J. H.; Takacs, C. J.; Seifter, J.; Heeger, A. J. *Adv. Mater.* **2011**, *23*, 1679−1683.
(6) Gadisa, A.; Liu, Y.; Samulski, E. T.; Lopez, R. *Appl. Phys. Lett.* **2012**, *100*, 253903(1)−253903(4).
(7) Waldauf, C.; Morana, M.; Denk, P.; Schilinsky, P.; Coakley, K.; Choulis, S. A.; Brabec, C. J. *Appl. Phys. Lett.* **2006**, *89*, 233517(1)−233517(3).
(8) Gilot, J.; Wienk, M. M.; Janssen, R. A. J. *Appl. Phys. Lett.* **2007**, *90*, 143512(1)−143512(3).
(9) Murase, S.; Yang, Y. *Adv. Mater.* **2012**, *24*, 2459−2462.
(10) Zilberberg, K.; Trost, S.; Schmidt, H.; Riedl, T. *Adv. Energy Mater.* **2011**, *1*, 377−381.
(11) Seo, J.; Gutacker, A.; Sun, Y. M.; Wu, H. B.; Huang, F.; Cao, Y.; Scherf, U.; Heeger, A. J.; Bazan, G. C. *J. Am. Chem. Soc.* **2011**, *133*, 8416−8419.
(12) He, Z.; Zhong, C.; Huang, X.; Wong, W.-Y.; Wu, H.; Chen, L.; Su, S.; Cao, Y. *Adv. Mater.* **2011**, *23*, 4636−4643.
(13) You, J.; Chen, C.-C.; Dou, L.; Murase, S.; Duan, H.-S.; Hawks, S. A.; Xu, T.; Son, H. J.; Yu, L.; Li, G.; Yang, Y. *Adv. Mater.* **2012**, *24*, 5267−5272.
(14) Deroubaix, G.; Marcus, P. *Surf. Interface Anal.* **1992**, *18*, 39−46.
(15) (a) Carley, A. F.; Chalker, P. R.; Riviere, J. C.; Roberts, M. W. *J. Chem. Soc., Faraday Trans. 1* **1987**, *83*, 351−370. (b) Pouilleau, J.; Devilliers, D.; Groult, H.; Marcus, P. *J. Mater. Sci.* **1997**, *32*, 5645−5651.
(16) (a) Jiang, X.; Wong, F. L.; Fung, M. K.; Lee, S. T. *Appl. Phys. Lett.* **2003**, *83*, 1875−1877. (b) Park, S.-M.; Ikegami, T.; Ebihara, K. *Jpn. J. Appl. Phys.* **2006**, *45*, 8453−8456. (c) Kim, T. W.; Choo, D. C.; No, Y. S.; Choi, W. K.; Choi, E. H. *Appl. Surf. Sci.* **2006**, *253*, 1917−1920.
(17) Ellmer, K.; Klein, A.; Rech, B. *Springer Series in Materials Science*, Vol. *104*; Hull, R., Parisi, J., Osgood, R. M., Warlimont, H., Eds.; Springer: Heidelberg, Germany, 2008; Chapter 4.
(18) Wang, W.; Feng, Q.; Jiang, K.; Huang, J.; Zhang, X.; Song, W.; Tan, R. *Appl. Surf. Sci.* **2011**, *257*, 3884−3887.
(19) Sugiyama, K.; Ishii, H.; Ouchi, Y.; Seki, K. *J. Appl. Phys.* **2000**, *87*, 295−298.
(20) Ma, H.; Yip, H.-L.; Huang, F.; Jen, A. K.-Y. *Adv. Funct. Mater.* **2010**, *20*, 1371−1388.
(21) Kim, J. Y.; Lee, K.; Coates, N. E.; Moses, D.; Nguyen, T.-Q.; Dante, M.; Heeger, A. J. *Science* **2007**, *317*, 222−225.
(22) (a) Ma, W.; Yang, C.; Gong, X.; Lee, K.; Heeger, A. J. *Adv. Funct. Mater.* **2005**, *15*, 1617−1622. (b) Li, G.; Shrotriya, V.; Huang, J.; Yao, Y.; Moriarty, T.; Emery, K.; Yang, Y. *Nat. Mater.* **2005**, *4*, 864−868.
(23) Kyaw, A. K. K.; Wang, D. H.; Gupta, V.; Zhang, J.; Chand, S.; Bazan, G. C.; Heeger, A. J. *Adv. Mater.* **2013**, *25*, 2397−2402.
(24) Liu, J.; Shao, S.; Meng, B.; Fang, G.; Xie, Z.; Wang, L.; Li, X. *Appl. Phys. Lett.* **2012**, *100*, 213906(1)−213906(3).
(25) Lim, D. C.; Kim, K.-D.; Park, S.-Y.; Hong, E. M.; Seo, H. O.; Lim, J. H.; Lee, K. H.; Jeong, Y.; Song, C.; Lee, E.; Kim, Y. D.; Cho, S. *Energy Environ. Sci.* **2012**, *5*, 9803−9807.
(26) Park, H.-Y.; Lim, D.; Kimb, K.-D.; Jang, S.-Y. *J. Mater. Chem. A* **2013**, *1*, 6327−6334.
(27) Li, N.; Stubhan, T.; Baran, D.; Min, J.; Wang, H.; Ameri, T.; Brabec, C. J. *Adv. Energy Mater.* **2013**, *3*, 301−307.